

## Bulk electronic structure of Ni<sub>2</sub>MnGa studied by density functional theory and hard x-ray photoelectron spectroscopy

Joydipto Bhattacharya,<sup>1,2,\*</sup> Pampa Sadhukhan<sup>3,\*</sup> Shuvam Sarkar<sup>3</sup>, Vipin Kumar Singh<sup>3</sup>, Andrei Gloskovskii,<sup>4</sup> Sudipta Roy Barman<sup>1</sup> and Aparna Chakrabarti<sup>1,2</sup>

<sup>1</sup>Homi Bhabha National Institute, Training School Complex, Anushakti Nagar, Mumbai 400094, Maharashtra, India

<sup>2</sup>Raja Ramanna Centre for Advanced Technology, Indore 452013, Madhya Pradesh, India

<sup>3</sup>UGC-DAE Consortium for Scientific Research, Khandwa Road, Indore 452001, Madhya Pradesh, India

<sup>4</sup>Deutsches Elektronen-Synchrotron DESY, Notkestrasse 85, D-22607 Hamburg, Germany



(Received 23 March 2023; revised 27 July 2023; accepted 1 September 2023; published 29 September 2023)

A combined study employing density functional theory (DFT) using the experimentally determined modulated structures in the martensite phase and bulk-sensitive hard x-ray photoelectron spectroscopy of stoichiometric single-crystalline Ni<sub>2</sub>MnGa is presented in this paper. The experimental valence band (VB) features closely match the theoretical VB calculated by DFT using generalized gradient approximation for both the martensite and austenite phases. We establish the existence of a charge density wave (CDW) state in the martensite phase from the shape of the VB near the Fermi level ( $E_F$ ). This shows (i) a transfer of spectral weight from the near  $E_F$  region to the higher binding energy side resulting in a dip-peak structure in the difference spectrum that is in excellent agreement with DFT and (ii) presence of a pseudogap at  $E_F$  that is portrayed by fitting the near  $E_F$  region with a power-law function. The present paper emphasizes the electronic origin and the role of the atomic modulation in hosting the CDW state in the martensite phase of stoichiometric Ni<sub>2</sub>MnGa.

DOI: [10.1103/PhysRevB.108.L121114](https://doi.org/10.1103/PhysRevB.108.L121114)

In recent years, considerable research has focused on understanding the intriguing physical phenomena connected to the charge density wave (CDW) state [1–5]. CDW is a collective excitation with periodic lattice distortion or modulation that often results in a pseudogap at  $E_F$  [6–8] and has been observed in various chalcogenide systems [9–11]. Ni<sub>2</sub>MnGa is an intriguing Heusler alloy having topologically protected nontrivial spin structures, such as skyrmions [12], where the nature of atomic rearrangements related to the existence of a bulk CDW state in the martensite phase has been a topic of intense study over the past three decades, but remains unresolved to date [13–30]. In addition, Ni<sub>2</sub>MnGa is of practical importance due to its large magnetocaloric effect [31,32] and magnetic field induced strain of approximately 10% [33,34], the latter of which has been correlated with its large magnetocrystalline anisotropy [35] and low twinning stress in the low-temperature martensite phase.

It was observed quite early on that the martensite phase is not a simple tetragonal distortion of the high-temperature cubic (austenite) phase; rather, the structure has a periodic modulation. Using powder neutron diffraction, Brown *et al.* could account for all the reflections using a sevenfold supercell (7M) with a commensurate wave vector [ $q_{\text{CDW}}$ ] of  $\frac{3}{7}c^*$ , i.e.,  $0.4286c^*$  [14]. The modulation results from a periodic shuffling of (110) planes of the cubic phase along the [110] direction. Later, structural studies using high resolution x-ray diffraction (XRD) [15,16] showed that the martensite phase has a sinusoidal modulation in the positions of all the three elemental constituents indicating formation of CDW with  $q_{\text{CDW}}$

of  $0.425c^*$ . Significantly, from inelastic neutron diffraction study [21], the martensite phase was reported to be distorted by transverse modulation with incommensurate wave vector close to that reported from XRD [15,16] that was attributed to electron-phonon interactions and anharmonic effects. A phason excitation was observed in the martensite phase of Ni<sub>2</sub>MnGa from a neutron scattering experiment that was related to a CDW state [20]. Evidence of modulation in the martensite phase of Ni<sub>2</sub>MnGa was also observed in electron and x-ray diffraction studies from the appearance of the satellite spots [17,25,26], as is well-known for chalcogenide materials that exhibit CDW [36,37]. From an ultraviolet photoemission spectroscopy (UPS) study [13], the existence of CDW in the premartensite phase [38] was shown on the surface of Ni<sub>2</sub>MnGa(100) that continued to exist also in the martensite phase. However, UPS being a highly surface sensitive technique with inelastic mean free path (IMFP) of 5 Å, the presence of CDW could not be inferred for the bulk martensite phase and the role of modulation was not probed. A time-resolved experiment identified a coherent phonon that was related to the amplitude of the modulated structure [23]. From an *ab initio* theoretical study, Bungaro *et al.* revealed that the dynamical instability in the TA<sub>2</sub> phonon mode is connected with the nesting of the Fermi surface [18], which is regarded as the distinguishing feature of the CDW state. Another first-principles study by Zayak *et al.* reported that the martensite phase is stabilized by modulation that showed a tendency to exhibit a pseudogap [19]; the modulated structure was close to that reported in Ref. [17].

Structural studies show that antisite defects and disorder are not present in Ni<sub>2</sub>MnGa [14–16]. The different nuclear scattering amplitudes of Ni, Mn, and Ga in neutron diffraction

\*These two authors contributed equally to this paper.

gave occupancies of 1 for all three atoms at their respective sites [14]. However, non-stoichiometry that can be induced in Ni-Mn-Ga by preparing specimens deviating from the 2:1:1 atomic ratio of stoichiometric Ni<sub>2</sub>MnGa influences its magnetic and structural properties as well as the transition temperatures [39–45]. For example, while the martensite start temperature ( $T_M$ ) is around 206 K for stoichiometric Ni<sub>2</sub>MnGa, it increases for Ni excess compositions to as large as 537 K for  $x = 0.35$  in Ni<sub>2+x</sub>Mn<sub>1-x</sub>Ga [40,41]. In contrast, the Curie temperature (376 K for  $x = 0$ ) decreases with increasing Ni content and for  $x \sim 0.2$  becomes equal to  $T_M$  [40,41].

Turning to the structural properties, in contrast to stoichiometric Ni<sub>2</sub>MnGa, where modulated structure is observed [14–16], for non-stoichiometric Ni<sub>2.19</sub>Mn<sub>0.88</sub>Ga<sub>0.93</sub>, i.e.,  $x = 0.19$ , the structure is tetragonal and modulation is not observed [28,41]. For this composition, a 14M nanotwin model of the adaptive martensite phase was suggested by Kaufmann *et al.* [28]. Similarly, the signature of nanotwins from transmission electron microscopy was obtained for non-stoichiometric compositions that exhibit martensite phase at room temperature [27], whereas Ni<sub>2</sub>MnGa exhibits the martensite phase below  $T_M$  ( $= 206$  K) [46]. Our survey of literature indicates that in compositions where the martensite phase has a nonmodulated tetragonally distorted Bain transition, the adaptive phase model [28] is applicable. However, a relatively recent density functional theory (DFT) calculation shows that even for stoichiometric Ni<sub>2</sub>MnGa, the modulation originates from the nanotwin ordering [29]. The authors establish that the phonon softening in the cubic austenite phase initializes the movement of the lattice planes, which seamlessly results in a nanotwinned adaptive martensite phase. However, this proposition is not supported by the conclusions of a large number of theoretical and experimental studies discussed above [13–26]. In particular, the nanotwin structure [28] was ruled out for stoichiometric Ni<sub>2</sub>MnGa from a high-resolution XRD study based on inhomogeneous displacements of the different atomic sites and the presence of phason broadening [16]. In spite of the above-mentioned studies indicating formation of a CDW in bulk Ni<sub>2</sub>MnGa [13–26], a very recent theoretical study on Ni<sub>2</sub>MnGa using a quasiparticle self-consistent GW (QSGW) method supports the formation of the 14M nanotwinned phase and thus raises doubts about the existence of the periodic modulation and the CDW state in this system [30].

In this paper, using a combination of DFT and hard x-ray photoelectron spectroscopy (HAXPES), we investigate the bulk electronic structure of Ni<sub>2</sub>MnGa to settle the aforementioned disagreement in the literature. We perform DFT calculations utilizing the actual experimental structures [14–16], unlike previous theoretical investigations that used only nonmodulated and model structures [19,29,30,47,48]. We also conducted DFT calculations utilizing the model nanotwin structure [28] to compare with the modulated structures. Due to the development of high-brilliance synchrotron sources working in the stable top-up mode [49], HAXPES has turned out to be a useful technique to probe the bulk electronic structure [50–55]. Although there are a few HAXPES studies on other Heusler alloys [56–58], the only work on Ni-Mn-Ga system is a comparison of two non-stoichiometric compositions [59]. Thus, this paper is not related to our cur-

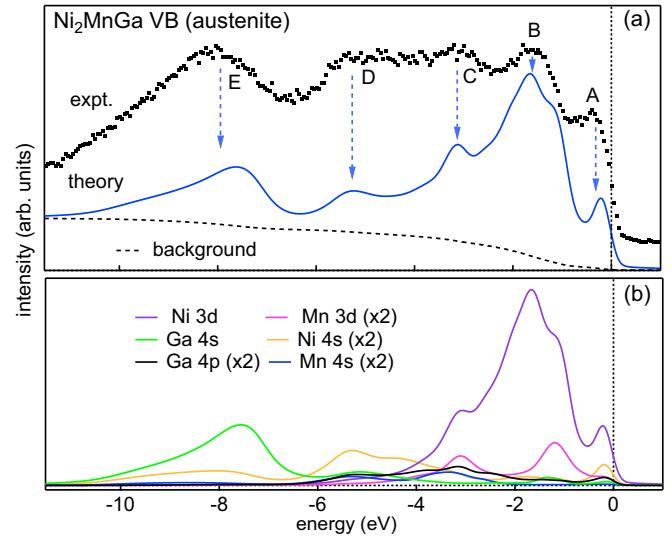


FIG. 1. (a) The experimental HAXPES VB spectra of Ni<sub>2</sub>MnGa in the austenite phase taken with 6 keV photon energy at 300 K compared with the theoretical VB spectrum calculated from the partial DOS. Features A–E are marked by blue dashed arrows. The zero in the energy scale corresponds to the Fermi level ( $E_F$ ). (b) The partial atom and orbital projected components of the theoretical VB.

rent investigation on stoichiometric Ni<sub>2</sub>MnGa in the austenite (300 K) and martensite phase (50 K) employing HAXPES and also DFT. In fact, the HAXPES study of the valence band (VB), in particular, near the Fermi level ( $E_F$ ), would not only throw light on the CDW state but also act as the gold standard for the DFT results to ascertain which structure best characterizes the martensite phase of Ni<sub>2</sub>MnGa.

*HAXPES and DFT VB spectra in the austenite phase.* In Fig. 1(a), we compare the theoretical and experimental VBs for the austenite phase of Ni<sub>2</sub>MnGa with L2<sub>1</sub> structure [60] (see Table S1 for its structural parameters, also Fig. S1 of the Supplemental Material (SM) [61] for the structure). The HAXPES VB spectrum exhibits five distinct features at about  $-0.25$  (A),  $-1.6$  (B),  $-3.2$  (C),  $-5.35$  (D), and  $-8$  eV (E). These features are the signatures of the bulk electronic structure since HAXPES is a bulk-sensitive technique with an IMFP of 66 Å (84 Å) at 6 (8) keV [62].

To compare with the experiment, we have calculated the VB spectrum considering the *s*, *p*, and *d* orbital projected components of the partial density of states (PDOS) of Ni, Mn, and Ga considering their respective photoemission cross sections [63] (see the Methods section in the SM [61] and see also Refs. [14–17] therein). In Fig. 1(b), some of the dominant partial contributions to the calculated total VB spectrum [blue curve in Fig. 1(a)] are shown. As shown by the blue dashed arrows in Fig. 1(a), the energy positions of the features in the experimental spectra are in good agreement with the calculated VB spectra.

The sharp peak shown by A corresponds to the feature  $a_1$ , observed in the theoretical density of states (DOS), see Note A and Fig. S2 in the SM [61]. This arises due to the Ni 3*d* minority states, with some admixture of the Ni 4*s* states, with minor contribution from Mn and Ga states. The intense peak B is dominated by Ni 3*d* majority and minority spin

states, which corresponds to feature  $c_1$  at  $-1.7$  eV. A hump is observed at the lower binding energy side of B [feature  $b_1$ ] at about  $-1.1$  eV. This has major contributions from Mn  $3d$  majority spin states and also from the Ni  $3d$  states in both spin channels. Feature C is primarily due to the Ni  $3d$  states, with significant contributions from the Mn  $3d$  up states; additionally, Ga  $4p$  and Ni as well as Mn  $4s$  states also contribute. While E has a dominant contribution from Ga  $4s$ , with some admixture of Ni  $4s$  states, D mainly arises from Ni  $4s$  states hybridized with Ga  $4s$ , Mn  $4s$ , and Ga  $4p$  states. Additionally, a peak observed in the unoccupied states around  $1.45$  eV (Fig. S2 of the SM [61]) arises primarily from the minority spin Mn  $3d$  states, whose position is in good agreement with the inverse photoemission spectra [64].

A comparison of the HAXPES spectra taken with 8 and 6 keV shows that all features A–E occur at similar energies (Fig. S3 of the SM [61]). Note that the larger photoemission cross-section of the  $s$  states in HAXPES leads to the appearance of features C–E in contrast to low-energy phototemission such as x-ray photoelectron spectroscopy (XPS), where C and D are not visible and E is weak [46]. In Fig. S3 of the SM [61], feature B appears at almost the same energy in XPS and HAXPES. This indicates that the recoil effect [65]—a phenomenon observed in HAXPES of light materials [66] as a shift of the photoemission peaks to higher binding energy—is not significant. In addition, as is the case for Ni<sub>2</sub>MnGa, the recoil effect has been reported to be insignificant for heavier  $3d$  transition metal systems [52–54,58].

It is noteworthy that, according to a recent QSGW calculation [30], the austenite phase exhibits a peak right at  $E_F$  in the minority spin DOS. This is in disagreement with our present (feature  $a_1$  in Fig. S2(a) of the SM [61]) as well as previous DFT results [19,47,48,67]. These DFT studies using the generalized gradient approximation (GGA) exchange-correlation functional (XC) observed that this peak appears between  $-0.19$  to  $-0.22$  eV, which agrees nicely with feature A of the HAXPES VB. In light of the good agreement between the results of DFT calculation performed with GGA XC and the HAXPES data (Fig. 1), it can be argued that the GGA XC quite accurately describes the electronic structure of Ni<sub>2</sub>MnGa. This justifies its use for the in-depth investigation of the martensite phase that has complicated modulated structures with a large unit cell [14–16].

*VB spectra in the Martensite phase.* In the literature, the first structural refinement of Ni<sub>2</sub>MnGa was carried out by Brown *et al.* [14] who reported  $q_{\text{CDW}} = \frac{2}{7}c^*$  with sinusoidal modulations for both Ni and Mn atoms, while Ga shows a nonsinusoidal modulation (see Table S2 of the SM [61] and Fig. 8(b) of Ref. [14]). The structure is shown in Fig. S1(b) of Supplemental Material [61] and henceforth referred to as modulated-Brown (in short, MDL-B). Righi *et al.* reported an incommensurate  $q = 0.4248(2)c^*$  (Table I, Ref. [15]) that can be approximated to a sevenfold supercell structure (see Fig. S1(c) and Table S3 of the SM [61] for structural parameters). However, the authors estimated that their  $q_{\text{CDW}}$  is closer to  $0.4c^*$  [ $= \frac{2}{5}c^*$ ] and called it a 5M structure. In this paper, the name MDL-R has been attributed to this (modulated-Righi) structure. In contrast to MDL-B, in the MDL-R structure the amplitude and phase of modulation of all the atoms were similar (Fig. S4 of SM [61]). Moreover, it was

TABLE I. Formation energy (in eV/atom) and magnetic moment values (in  $\mu_B$  per f.u.) obtained from DFT calculations for different structures of Ni<sub>2</sub>MnGa in the martensite phase.

Structure	Formation energy	Magnetic moment
MDL-B	-4.0325	3.94
MDL-R	-4.1783	4.21
MDL-S	-4.1927	4.20
NTN-K	-4.1837	4.20

pointed out that the MDL-B structure contains some Ni-Mn and Ni-Ga distances— $2.09$  and  $2.06$  Å, respectively—that are unexpectedly short [15]. Singh *et al.* found higher-order satellite reflections up to the third order and phason broadening of the satellite peaks in their XRD pattern and their refinement with the same superspace group as Righi *et al.* gave  $q_{\text{CDW}} = 0.4316(3)c^*$ , which was approximated to a sevenfold supercell structure with similar atomic modulations like the MDL-R structure and with a  $q_{\text{CDW}}$  value of  $\frac{3}{7}c^*$  (see Table IV, Ref. [16]). This structure was referred to as 7M and is referred to henceforth as a modulated-Singh (MDL-S) structure (see Fig. S1(d) and Table S4 of SM [61]). Here, we have performed DFT calculations for all three above-discussed structures (MDL-B, MDL-R, and MDL-S). We have also considered the nanotwin structure which comprises a periodic twinning, i.e.,  $(5\bar{2})_2$ , of the tetragonal nonmodulated building blocks. Since this is a model structure, we have performed a full relaxation in our DFT calculation and this is referred to as nanotwin-Kaufmann (NTN-K) structure as shown in Fig. S1(e) and Table S5 of the SM [61].

Table I shows that for all structures, although both the total energy and magnetic moment are rather close to each other, the MDL-S structure has the lowest energy showing that it is the most stable one. The spin-integrated total DOS (TDOS) and the PDOS for all the above-mentioned structures—as well as the calculated VB along with some partial components—are shown in Figs. S5–S8 and discussed in Note B of the SM [61]. In Fig. 2, we compare the calculated VB spectra for the above structures with the experiment. The suppression and shift of feature A to  $-0.6$  eV in the martensite phase compared to  $-0.25$  eV in the austenite phase (Fig. 1) in the HAXPES VB is nicely reproduced by the MDL-R and MDL-S (MDL-R/S) structures (Fig. 2), feature A is over suppressed in MDL-B and is nearly absent in NTN-K. Further, we observe that the features close to  $E_F$  are dominated by the down-spin states in the case of the MDL-R/S structures, but for the MDL-B and NTN-K cases, these have significant contributions from both spin channels (Fig. S2 [61]). Feature B is observed at the same energy position ( $\sim -1.5$  eV as shown by the blue dashed arrow) in all structures except for MDL-B, where it is shifted considerably to about  $-2$  eV. Thus, the MDL-B structure does not show good agreement with experiments, and this could be related to unphysically short Ni-Mn and Ni-Ga distances [15]. While features C–E are well reproduced in all the modulated structures, NTN-K shows an extra feature at  $-2.6$  eV (red arrow), related to Ni  $3d$  minority spin states, that is absent in the experiment. Thus, overall the NTN-K structure does not show good agreement

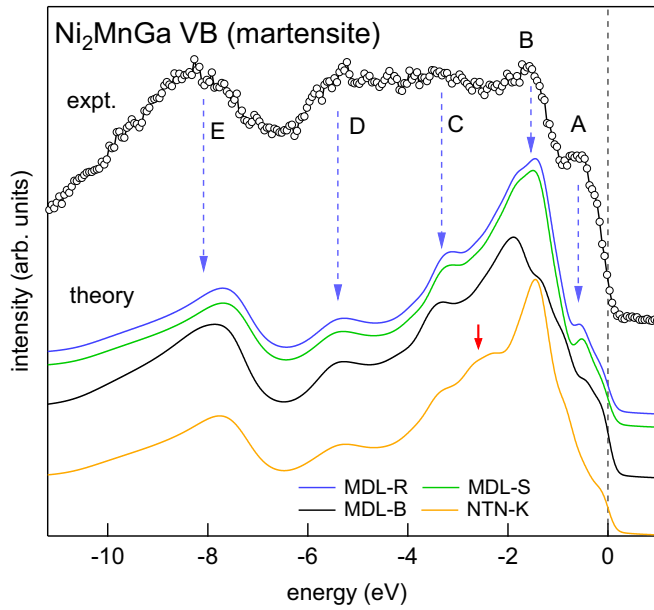


FIG. 2. Theoretical VB spectra of  $\text{Ni}_2\text{MnGa}$  calculated for the different sevenfold modulated structures (MDL-R, MDL-S, and MDL-B) and the nanotwin structure (NTN-K). These are staggered along the vertical axis and compared with the experimental VB spectrum in the martensite phase at 50 K.

indicating that the adaptive martensite model is not valid for stoichiometric  $\text{Ni}_2\text{MnGa}$ .

From the above discussions, it is evident that the theoretical VB spectra based on the MDL-R/S structures are in very good agreement with the experimental results, and hence only these will be considered moving forward. In fact, the VB spectra and the DOS of these two structures are quite similar (compare Figs. S6 and S7 [61]), which is related to the closeness of their crystal structure (compare Tables S3 and S4 of the SM [61]).

We investigated the effect of electron-electron Coulomb interaction [68] in  $\text{Ni}_2\text{MnGa}$  using GGA+ $U$  calculations with the MDL-S structure considering  $U$  at both Mn ( $U_{\text{Mn}}$ ) and Ni ( $U_{\text{Ni}}$ ) sites. With a small  $U_{\text{Mn}}$  value of 0.5 eV and  $U_{\text{Ni}} = 0$ , we find that the agreement with feature B of the VB spectrum improves (Fig. S9 of the SM [61]). However, larger  $U_{\text{Mn}}$  and  $U_{\text{Ni}}$  values of 1.8 to  $\sim 4$  eV reported in literature [69–71] disagree with the experimental VB spectrum as well as the reported saturation magnetization values ( $4.04 - 4.27 \mu_B$ ) [60,72–74] (see Note C and Figs. S9 and S10 of the SM [61]).

In addition, although antisite disorder is not reported in stoichiometric  $\text{Ni}_2\text{MnGa}$  from diffraction studies [14–16], we investigate the effect of 7% antisite disorder by exchanging a Mn atom with a Ni or Ga atom in the MDL-S structure having 14 Mn atoms in its 56-atom unit cell. The DOS in Fig. S11 of the SM [61] demonstrates that antisite disorder does not alter the position of the features, although it does slightly broaden them, as was previously observed in other ternary materials [58,75] (see also Refs. [30–32] of the SM [61]).

**CDW state in the martensite phase.** The top panel of Fig. 3(a) compares the experimental VB spectrum of the martensite and austenite phases. An interesting difference is observed between  $E_F$  and  $-1$  eV: In the martensite phase,

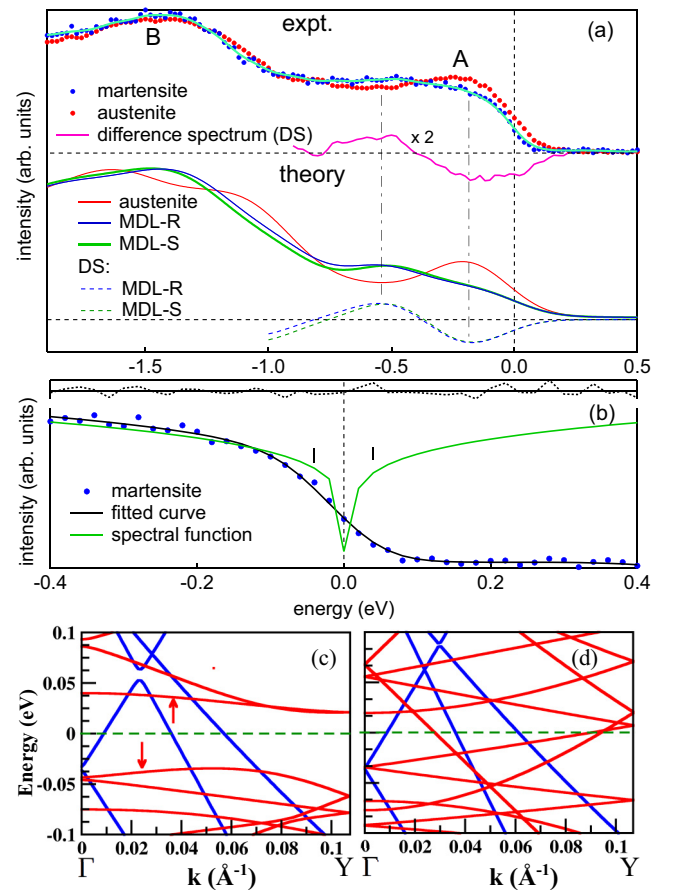


FIG. 3. (a) HAXPES VB of the martensite (50 K) and austenite (300 K) phases of  $\text{Ni}_2\text{MnGa}$  in the near  $E_F$  region (top panel) taken with small data steps. The cyan curve represents the martensite spectrum thermally broadened to 300 K. The bottom panel shows the theoretical VB spectra of the austenite, MDL-R/S martensite structures. Comparison of the dip and peak positions of the difference spectra (DS) between experiment (pink curve) and theory (dashed curves) shown by the dot-dashed vertical lines. (b) The VB spectrum of the martensite phase around  $E_F$  (blue filled circles) fitted (black curve) with a power law spectral function [82] (green). The residual is shown in the top panel. The band structure (red: minority; blue: majority spin) along the  $\mathbf{q}_{\text{CDW}}$  for the (c) MDL-S and the (d) non-modulated NMDL-S structures.

feature A is clearly suppressed, while an increased intensity around  $-0.55$  eV is observed in comparison to the austenite phase. However, feature B, as well as features C–E from Figs. 1 and 2 do not exhibit any noticeable difference. This indicates that the states close to  $E_F$  are influenced by the phase transition.

As the thermal broadening of the Fermi function increases with temperature, we convoluted the low-temperature (50 K) martensite spectrum with a Gaussian function of full width at half maximum of  $4k_B\Delta T$  [76] to obtain the difference spectra [DS = (martensite – austenite), top panel in Fig. 3(a)] unaffected by this effect. Here  $\Delta T = \sqrt{T_1^2 - T_2^2}$ ,  $T_1 = 300$  K,  $T_2 = 50$  K, and  $k_B$  is the Boltzmann constant. The DS spectrum exhibits a dip centered around  $-0.1$  eV and a peak at about  $-0.55$  eV. This characteristic dip-peak shape points to a transfer of spectral weight from  $-0.1$  eV to  $-0.55$  eV, which

is known to be a manifestation of the CDW state that has been observed in other systems [77–80]. In addition, the suppression of states at  $E_F$  in the martensite phase is more than 30%, indicating the creation of a pseudogap, which in turn also suggests a CDW state [6,8]. To confirm this, the shape of the spectrum near  $E_F$  needs to be determined because, according to the theoretical formulation of CDW [6,81], it should follow a power-law function [82] where  $\alpha$  is the exponent. This function was used to fit the near  $E_F$  spectrum of the martensite phase using a least-squares error minimization approach, where multiple starting values were applied and all parameters were adjusted, with the exception of the instrumental resolution. A random variation of the residual in the top panel of Fig. 3(b) shows that the fitting is satisfactory.

Interestingly, the power-law function portrays the pseudogap at  $E_F$ , and its width is estimated to be 80 meV from the separation between the inflection points shown by the black ticks.  $\alpha$  determines the shape of the spectral function, its value turns out to be  $0.18 \pm 0.02$ , which is close to that reported (0.16) for the surface CDW of Ni<sub>2</sub>MnGa in the martensite phase probed using surface-sensitive ( $< 5 \text{ \AA}$ ) UPS [13]. This shows that the CDW has a similar nature in the bulk and the surface. This is also supported by the similarity of  $q_{\text{CDW}}$  value obtained from the surface sensitive low energy electron diffraction study [25] and the bulk value from XRD.

Having shown in Fig. 2 that the MDL-R/S structures best describe the position of all features A–E of the experimental VB spectrum in the martensite phase, we examine whether the transfer of spectral weight is observed from DFT. In the lower panel of Fig. 3(a), the theoretical DS for both MDL-S and MDL-R show excellent agreement—as highlighted by the dot-dashed vertical lines—in both position and shape of the dip and the peak compared to the experiment in the upper panel. Thus, the transfer of spectral weight is nicely depicted by the DOS from DFT.

In Figs. 3(c) and 3(d), the band dispersion calculated along  $\mathbf{q}_{\text{CDW}}$ , i.e.,  $\Gamma Y$  for the MDL-S structure is compared to the nonmodulated structure (NMDL-S). The amplitude of modulation set to zero in NMDL-S, as shown in Fig. S12 of the SM [61]. Red arrows show an energy gap of 0.07–0.09 eV in the minority spin band of MDL-S. In contrast, NMDL-S does not exhibit any gap. This difference is thus directly related to the modulated CDW state. The minority spin band that exhibits the gap becomes relatively flat around  $-0.05 \text{ eV}$  [Fig. 3(c)]. This would result in an increase in the DOS around this energy and a decrease closer to the  $E_F$  that can explain the transfer of spectral weight [Fig. 3(a)]. On the other hand, the bands are nearly similar between MDL-S and NMDL-S along other directions, e.g., along  $\Gamma X$  and  $\Gamma Z$  and both spin bands cross  $E_F$  (Fig. S13 of the SM [61]). This results in a finite DOS at  $E_F$ , (Fig. S2 of the SM [61]), indicating presence of a Fermi edge in the photoemission spectrum. On the other hand, the pseudogap observed in the photoemission spectrum is

attributed to a many-body effect, which includes the electron-phonon coupling [8] that is not taken into consideration in our calculation.

*Conclusion.* A combined experimental and theoretical investigation of the bulk electronic structure of stoichiometric Ni<sub>2</sub>MnGa has been performed using HAXPES and DFT. The DFT calculations have been conducted for the modulated structures of the martensite phase as reported by previous diffraction studies, e.g., MDL-R/S [15,16] as well as the austenite phase with the L2<sub>1</sub> structure. Furthermore, the nanotwin model structure (NTN-K) [28] was considered. A comparison of the theoretical VB spectra for the different martensite phase structures with HAXPES VB spectrum reveals a very good feature to feature agreement in peak position and relative intensity for the MDL-R/S structures. In contrast, the NTN-K structure exhibits unsatisfactory agreement. This shows that the modulation determined from diffraction studies [15,16] correctly describes the electronic structure of the martensite phase of Ni<sub>2</sub>MnGa. A power-law function fits the HAXPES VB close to  $E_F$ , revealing an 80 meV pseudogap. Additionally, a transfer of spectral weight occurs from the near  $E_F$  region to the higher binding energy side, resulting in a dip-peak structure in the difference spectrum (DS). A minority spin band exhibits a gap at  $E_F$  in the CDW state along the  $q_{\text{CDW}}$  direction that can explain the transfer of spectral weight observed. The pseudogap and the transfer of spectral weight establish the existence of CDW in the martensite phase of Ni<sub>2</sub>MnGa. The excellent agreement in the DS between experiment and the theory for the MDL-R/S structures show the role of the periodic atomic modulation in achieving the CDW state. Our calculations indicate that GGA is adequate for describing the electronic structure of Ni<sub>2</sub>MnGa if the correct structure is considered and large values of  $U$  (1.8 to  $\sim 4 \text{ eV}$ ) suggested recently [69–71] contradict the experimental results. Our paper establishes the electronic origin and the role of the atomic modulation in hosting the CDW state in the martensite phase of stoichiometric Ni<sub>2</sub>MnGa and resolves a recently generated controversy [29,30,69].

*Acknowledgments.* J.B. and A.C. thank the director, RRCAT, for facilities and encouragement, and A. Banerjee and T. Ganguli for discussions. RRCAT computer division is thanked for the installation of the software and support. J.B. thanks RRCAT and HBNI for financial support. The HAXPES experiments were carried out at PETRA III of Deutsches Elektronen-Synchrotron, a member of Helmholtz-Gemeinschaft Deutscher Forschungszentren. Financial support by the Department of Science and Technology, Government of India within the framework of India@DESY collaboration is gratefully acknowledged. T. A. Lograsso and D. L. Schlager are thanked for providing us with the single crystal specimen. We are thankful to C. Schlueter and K. Biswas for support and encouragement. We would like to acknowledge the skillful technical support from K. Ederer.

[1] Y. Wang, I. Petrides, G. McNamara, Md. M. Hosen, S. Lei, Y-C. Wu, J. L. Hart, H. Lv, J. Yan, D. Xiao *et al.*, Axial higgs mode detected by quantum pathway interference in RTe<sub>3</sub>, *Nature (London)* **606**, 896 (2022).

[2] H. Pan, M. Xie, F. Wu, and S. Das Sarma, Topological Phases in AB-Stacked MoTe<sub>2</sub>/WSe<sub>2</sub>: Z<sub>2</sub> Topological Insulators, Chern Insulators, and Topological Charge Density Waves, *Phys. Rev. Lett.* **129**, 056804 (2022).

- [3] Y.-X. Jiang, J.-X. Yin, M. M. Denner, N. Shumiya, B. R. Ortiz, G. Xu, Z. Guguchia, J. He, Md. S. Hossain, X. Liu *et al.*, Unconventional chiral charge order in kagome superconductor  $KV_3Sb_5$ , *Nat. Mater.* **20**, 1353 (2021).
- [4] W. Shi, B. J. Wieder, H. L. Meyerheim, Y. Sun, Y. Zhang, Y. Li, L. Shen, Y. Qi, L. Yang, J. Jena *et al.*, A charge-density-wave topological semimetal, *Nat. Phys.* **17**, 381 (2021).
- [5] A. Zong, A. Kogar, Y.-Q. Bie, T. Rohwer, C. Lee, E. Baldini, E. Ergeçen, M. B. Yilmaz, B. Freelon, E. J. Sie *et al.*, Evidence for topological defects in a photoinduced phase transition, *Nat. Phys.* **15**, 27 (2019).
- [6] R. H. McKenzie, Microscopic theory of the pseudogap and Peierls transition in quasi-one-dimensional materials, *Phys. Rev. B* **52**, 16428 (1995).
- [7] G. Grüner, The dynamics of charge-density waves, *Rev. Mod. Phys.* **60**, 1129 (1988).
- [8] P. A. Lee, T. M. Rice, and P. W. Anderson, Fluctuation Effects at a Peierls Transition, *Phys. Rev. Lett.* **31**, 462 (1973).
- [9] P. Walmsley, S. Aeschlimann, J. A. W. Straquadine, P. Giraldo-Gallo, S. C. Riggs, M. K. Chan, R. D. McDonald, and I. R. Fisher, Magnetic breakdown and charge density wave formation: A quantum oscillation study of the rare-earth tritellurides, *Phys. Rev. B* **102**, 045150 (2020).
- [10] J. Dai, E. Calleja, J. Alldredge, X. Zhu, L. Li, W. Lu, Y. Sun, T. Wolf, H. Berger, and K. McElroy, Microscopic evidence for strong periodic lattice distortion in two-dimensional charge-density wave systems, *Phys. Rev. B* **89**, 165140 (2014).
- [11] H. J. Kim, C. D. Malliakas, A. T. Tomić, S. H. Tessmer, M. G. Kanatzidis, and S. J. L. Billinge, Local Atomic Structure and Discommensurations in the Charge Density Wave of  $CeTe_3$ , *Phys. Rev. Lett.* **96**, 226401 (2006).
- [12] C. Phatak, O. Heinonen, M. D. Graef, and A. P.-Long, Nanoscale skyrmions in a nonchiral metallic multiferroic:  $Ni_2MnGa$ , *Nano Lett.* **16**, 4141 (2016).
- [13] S. W. D'Souza, A. Rai, J. Nayak, M. Maniraj, R. S. Dhaka, S. R. Barman, D. L. Schlagel, T. A. Lograsso, and A. Chakrabarti, Coexistence of charge-density wave and ferromagnetism in  $Ni_2MnGa$ , *Phys. Rev. B* **85**, 085123 (2012).
- [14] P. J. Brown, J. Crangle, T. Kanomata, M. Matsumoto, K.-U. Neumann, B. Ouladdiaf, and K. R. A. Ziebeck, The crystal structure and phase transitions of the magnetic shape memory compound  $Ni_2MnGa$ , *J. Phys.: Condens. Matter* **14**, 10159 (2002).
- [15] L. Righi, F. Albertini, G. Calestani, L. Pareti, A. Paoluzi, C. Ritter, P. A. Algarabel, L. Morellon, and M. R. Ibarra, Incommensurate modulated structure of the ferromagnetic shape-memory  $Ni_2MnGa$  martensite, *J. Solid State Chem.* **179**, 3525 (2006).
- [16] S. Singh, V. Petricek, P. Rajput, A. H. Hill, E. Suard, S. R. Barman, and D. Pandey, High-resolution synchrotron x-ray powder diffraction study of the incommensurate modulation in the martensite phase of  $Ni_2MnGa$ : Evidence for nearly 7M modulation and phason broadening, *Phys. Rev. B* **90**, 014109 (2014).
- [17] V. V. Martynov and V. V. Kokorin, The crystal structure of thermally- and stress-induced martensites in  $Ni_2MnGa$  single crystals, *J. Phys. III France* **2**, 739 (1992).
- [18] C. Bungaro, K. M. Rabe, and A. Dal Corso, First-principles study of lattice instabilities in ferromagnetic  $Ni_2MnGa$ , *Phys. Rev. B* **68**, 134104 (2003).
- [19] A. T. Zayak, P. Entel, J. Enkovaara, A. Ayuela, and R. M. Nieminen, First-principles investigations of homogeneous lattice-distortive strain and shuffles in  $Ni_2MnGa$ , *J. Phys.: Condens. Matter* **15**, 159 (2003).
- [20] S. M. Shapiro, P. Vorderwisch, K. Habicht, K. Hradil, and H. Schneider, Observation of phasons in the magnetic shape memory alloy  $Ni_2MnGa$ , *Europhys. Lett.* **77**, 56004 (2007).
- [21] A. Zheludev, S. M. Shapiro, P. Wochner, and L. E. Tanner, Precursor effects and premartensitic transformation in  $Ni_2MnGa$ , *Phys. Rev. B* **54**, 15045 (1996).
- [22] R. Chulist, C.-G. Oertel, W. Skrotzka, and T. Lippmann, Direction of modulation during twin boundary motion, *Scr. Mater.* **62**, 235 (2010).
- [23] S. O. Mariager, C. Dornes, J. A. Johnson, A. Ferrer, S. Greubel, T. Huber, A. Caviezel, S. L. Johnson, T. Eichhorn, G. Jakob, H. J. Elmers, P. Beaud, C. Quitmann, and G. Ingold, Structural and magnetic dynamics in the magnetic shape-memory alloy  $Ni_2MnGa$ , *Phys. Rev. B* **90**, 161103(R) (2014).
- [24] S. Singh, J. Bednarcik, S. R. Barman, C. Felser, and D. Pandey, Premartensite to martensite transition and its implications for the origin of modulation in  $Ni_2MnGa$  ferromagnetic shape-memory alloy, *Phys. Rev. B* **92**, 054112 (2015).
- [25] S. W. D'Souza, J. Nayak, M. Maniraj, A. Rai, R. S. Dhaka, S. R. Barman, D. L. Schlagel, T. A. Lograsso, and A. Chakrabarti,  $Ni_2MnGa(100)$  ferromagnetic shape memory alloy: A surface study, *Surf. Sci.* **606**, 130 (2012).
- [26] T. Fukuda, H. Kushida, M. Todai, T. Kakeshita, and H. Mori, Crystal structure of the martensite phase in the ferromagnetic shape memory compound  $Ni_2MnGa$  studied by electron diffraction, *Scr. Mater.* **61**, 473 (2009).
- [27] J. Pons, R. Santamarta, V. A. Chernenko, and E. Cesari, Modelling the phase diagram of magnetic shape memory Heusler alloys, *J. Appl. Phys.* **97**, 083516 (2005).
- [28] S. Kaufmann, U. K. Röbber, O. Heczko, M. Wuttig, J. Buschbeck, L. Schultz, and S. Fähler, Adaptive Modulations of Martensites, *Phys. Rev. Lett.* **104**, 145702 (2010).
- [29] M. E. Gruner, R. Niemann, P. Entel, R. Pentcheva, U. K. Röbber, K. Nielsch, and S. Fähler, Modulations in martensitic Heusler alloys originate from nanotwin ordering, *Sci. Rep.* **8**, 8489 (2018).
- [30] M. Obata, T. Kotani, and T. Oda, Intrinsic instability to martensite phases in ferromagnetic shape memory alloy  $Ni_2MnGa$ : Quasiparticle self-consistent GW investigation, *Phys. Rev. Mater.* **7**, 024413 (2023).
- [31] X. Zhou, W. Li, H. P. Kunkel, and G. Williams, A criterion for enhancing the giant magnetocaloric effect: (Ni-Mn-Ga)-a promising new system for magnetic refrigeration, *J. Phys.: Condens. Matter* **16**, L39 (2004).
- [32] J. Marcos, L. Mañosa, A. Planes, F. Casanova, X. Batlle, and A. Labarta, Multiscale origin of the magnetocaloric effect in Ni-Mn-Ga shape-memory alloys, *Phys. Rev. B* **68**, 094401 (2003).
- [33] A. Sozinov, A. A. Likhachev, N. Lanska, and K. Ullakko, Giant magnetic-field-induced strain in NiMnGa seven-layered martensitic phase, *Appl. Phys. Lett.* **80**, 1746 (2002).
- [34] S. J. Murray, M. Marioni, S. M. Allen, R. C. O'Handley, and T. A. Lograsso, 6% magnetic-field-induced strain by twin-boundary motion in ferromagnetic Ni-Mn-Ga, *Appl. Phys. Lett.* **77**, 886 (2000).
- [35] F. Casoli, G. Varvaro, M. T. Ghahfarokhi, S. Fabbri, and F. Albertini, Insight into the magnetisation process of martensitic

- Ni-Mn-Ga films: a micromagnetic and vector magnetometry study, *J. Phys.: Mater.* **3**, 045003 (2020).
- [36] E. DiMasi, M. C. Aronson, J. F. Mansfield, B. Foran, and S. Lee, Chemical pressure and charge-density waves in rare-earth tritellurides, *Phys. Rev. B* **52**, 14516 (1995).
- [37] S. Sarkar, J. Bhattacharya, P. Sadhukhan, D. Curcio, R. Dutt, V. K. Singh, M. Bianchi, A. Pariari, S. Roy, P. Mandal, T. Das, P. Hofmann, A. Chakrabarti, and S. R. Barman, Charge density wave induced nodal lines in LaTe<sub>3</sub>, *Nat. Commun.* **14**, 3628 (2023).
- [38] S. Singh, J. Nayak, A. Rai, P. Rajput, A. H. Hill, S. R. Barman, and D. Pandey, (3+1)D superspace description of the incommensurate modulation in the premartensite phase of Ni<sub>2</sub>MnGa: A high resolution synchrotron x-ray powder diffraction study, *J. Phys.: Condens. Matter* **25**, 212203 (2013).
- [39] Y. Sokolovskaya, O. Miroshkina, D. Baigutlin, V. Sokolovskiy, M. Zagrebin, V. Buchelnikov, and A. T. Zayak, A ternary map of Ni-Mn-Ga Heusler alloys from ab initio calculations, *Metals* **11**, 973 (2021).
- [40] A. N. Vasil'ev, A. D. Bozhko, V. V. Khovailo, I. E. Dikshstein, V. G. Shavrov, V. D. Buchelnikov, M. Matsumoto, S. Suzuki, T. Takagi, and J. Tani, Structural and magnetic phase transitions in shape-memory alloys Ni<sub>2+x</sub>Mn<sub>1-x</sub>Ga, *Phys. Rev. B* **59**, 1113 (1999).
- [41] S. Banik, R. Ranjan, A. Chakrabarti, S. Bhardwaj, N. P. Lalla, A. M. Awasthi, V. Sathe, D. M. Phase, P. K. Mukhopadhyay, D. Pandey, and S. R. Barman, Structural studies of Ni<sub>2+x</sub>Mn<sub>1-x</sub>Ga by powder x-ray diffraction and total energy calculations, *Phys. Rev. B* **75**, 104107 (2007).
- [42] S. Banik, S. Singh, R. Rawat, P. K. Mukhopadhyay, B. L. Ahuja, A. M. Awasthi, S. R. Barman, and E. V. Sampathkumaran, Variation of magnetoresistance in Ni<sub>2+x</sub>Mn<sub>1-x</sub>Ga with composition, *J. Appl. Phys.* **106**, 103919 (2009).
- [43] S. Singh, R. Rawat, and S. R. Barman, Existence of modulated structure and negative magnetoresistance in Ga excess Ni-Mn-Ga, *Appl. Phys. Lett.* **99**, 021902 (2011).
- [44] S. Banik, P. K. Mukhopadhyay, A. M. Awasthi, and S. R. Barman, Structural studies on Mn excess and Ga deficient Ni-Mn-Ga, *Adv. Mater. Res.* **52**, 109 (2008).
- [45] S. Singh, P. Kushwaha, F. Scheibel, H.-P. Liermann, S. R. Barman, M. Acet, C. Felser, and D. Pandey, Residual stress induced stabilization of martensite phase and its effect on the magnetostructural transition in Mn-rich Ni-Mn-In/Ga magnetic shape-memory alloys, *Phys. Rev. B* **92**, 020105(R) (2015).
- [46] S. W. D'Souza, R. S. Dhaka, A. Rai, M. Maniraj, J. Nayak, S. Singh, D. L. Schlagel, T. A. Lograsso, A. Chakrabarti, and S. R. Barman, Surface study of Ni<sub>2</sub>MnGa(100), *Mater. Sci. Forum* **684**, 215 (2011).
- [47] S. Fujii, S. Ishida, and S. Asano, Electronic structure and lattice transformation in Ni<sub>2</sub>MnGa and Co<sub>2</sub>NbSn, *J. Phys. Soc. Jpn.* **58**, 3657 (1989).
- [48] S. R. Barman, S. Banik, and A. Chakrabarti, Structural and electronic properties of Ni<sub>2</sub>MnGa, *Phys. Rev. B* **72**, 184410 (2005).
- [49] S. Shin, New era of synchrotron radiation: fourth-generation storage ring, *AAPPS Bull.* **31**, 21 (2021).
- [50] *Hard X-ray Photoelectron Spectroscopy*, edited by J. C. Woicik, Springer Series in Surface Sciences Vol. 59 (Springer International Publishing, Cham, Switzerland, 2016).
- [51] A. X. Gray, C. Papp, S. Ueda, B. Balke, Y. Yamashita, L. Plucinski, J. Minár, J. Braun, E. R. Ylvisaker, C. M. Schneider *et al.*, Probing bulk electronic structure with hard x-ray angle-resolved photoemission, *Nat. Mater.* **10**, 759 (2011); A. X. Gray, J. Minár, S. Ueda, P. R. Stone, Y. Yamashita, J. Fujii, J. Braun, L. Plucinski, C. M. Schneider, G. Panaccione *et al.*, Electronic Structure Changes Across the Metamagnetic Transition in FeRh via Hard X-Ray Photoemission, *Phys. Rev. Lett.* **108**, 257208 (2012); T. Ohtsuki, A. Chainani, R. Eguchi, M. Matsunami, Y. Takata, M. Taguchi, Y. Nishino, K. Tamasaku, M. Yabashi, T. Ishikawa *et al.*, Role of Ti 3d Carriers in Mediating the Ferromagnetism of Co:TiO<sub>2</sub> Anatase Thin Films, *ibid.* **106**, 047602 (2011); M. Sing, G. Berner, K. Goß, A. Müller, A. Ruff, A. Wetscherek, S. Thiel, J. Mannhart, S. A. Pauli, C. W. Schneider *et al.*, Profiling the Interface Electron Gas of LaAlO<sub>3</sub>/SrTiO<sub>3</sub> Heterostructures with Hard X-Ray Photoelectron Spectroscopy, *ibid.* **102**, 176805 (2009).
- [52] J. Nayak, M. Maniraj, A. Rai, S. Singh, P. Rajput, A. Gloskovskii, J. Zegenhagen, D. L. Schlagel, T. A. Lograsso, K. Horn, and S. R. Barman, Bulk electronic structure of quasicrystals, *Phys. Rev. Lett.* **109**, 216403 (2012).
- [53] V. K. Singh, M. Krajčí, S. Sarkar, M. Balal, S. Barman, P. Sadhukhan, A. Gloskovskii, M. Feuerbacher, C. Thomas, P. Ebert, E. Rotenberg, K. Horn, and S. Roy Barman, Electronic structure of Al<sub>3</sub>Mg<sub>2</sub> and Al<sub>13</sub>Fe<sub>4</sub> complex metallic alloys, *Phys. Rev. B* **105**, 205107 (2022).
- [54] S. Sarkar, P. Sadhukhan, V. K. Singh, A. Gloskovskii, K. Deguchi, N. Fujita, and S. R. Barman, Bulk electronic structure of high-order quaternary approximants, *Phys. Rev. Res.* **3**, 013151 (2021); S. Sarkar, M. Krajčí, P. Sadhukhan, V. K. Singh, A. Gloskovskii, P. Mandal, V. Fournée, M.-C. de Weerd, J. Ledieu, I. R. Fisher, and S. R. Barman, Anderson localization of electron states in a quasicrystal, *Phys. Rev. B* **103**, L241106 (2021).
- [55] P. Sadhukhan, S. W. D'Souza, V. K. Singh, R. S. Dhaka, A. Gloskovskii, S. K. Dhar, P. Raychaudhuri, A. Chainani, A. Chakrabarti, and S. R. Barman, Role of antisite disorder, electron-electron correlations, and a surface valence transition in the electronic structure of CeMnNi<sub>4</sub>, *Phys. Rev. B* **99**, 035102 (2019).
- [56] M. Ye, A. Kimura, Y. Miura, M. Shirai, Y. T. Cui, K. Shimada, H. Namatame, M. Taniguchi, S. Ueda, K. Kobayashi, R. Kainuma, T. Shishido, K. Fukushima, and T. Kanomata, Role of Electronic Structure in the Martensitic Phase Transition of Ni<sub>2</sub>Mn<sub>1+x</sub>Sn<sub>1-x</sub> Studied by Hard-X-Ray Photoelectron Spectroscopy and *Ab Initio* Calculation, *Phys. Rev. Lett.* **104**, 176401 (2010).
- [57] S. Ueda, Y. Miura, Y. Fujita, and Y. Sakuraba, Direct probing of temperature-independent bulk half-metallicity in Co<sub>2</sub>MnSi by spin-resolved hard x-ray photoemission, *Phys. Rev. B* **106**, 075101 (2022).
- [58] P. Sadhukhan, S. Sarkar, S. W. D'Souza, A. Gloskovskii, and S. R. Barman, Bulk electronic structure of Mn<sub>2</sub>NiGa using hard x-ray photoelectron spectroscopy and density functional theory, *Phys. Scr.* **98**, 055912 (2023).
- [59] A. Kimura, M. Ye, M. Taniguchi, E. Ikenaga, J. M. Barandiarán, and V. A. Chernenko, Lattice instability of Ni-Mn-Ga ferromagnetic shape memory alloys probed by hard x-ray photoelectron spectroscopy, *Appl. Phys. Lett.* **103**, 072403 (2013).

- [60] P. J. Webster, K. R. A. Ziebeck, S. L. Town, and M. S. Peak, Magnetic order and phase transformation in Ni<sub>2</sub>MnGa, *Philos. Mag.* **B 49**, 295 (1984).
- [61] See Supplemental Material at <http://link.aps.org/supplemental/10.1103/PhysRevB.108.L121114> for the austenite and martensite phase structures that are being considered to calculate the theoretical valence band (VB) spectra; details of methodology of calculation; details of the HAXPES measurement; calculation of theoretical VB spectra; discussion of total and partial DOS; results of DFT+U calculations; discussion of effect of disorder. The Supplemental Material contains Figs. S1–S13, Tables S1–S6, Discussions I–V, and includes Refs. [83–96] of the main text.
- [62] S. Tanuma, C. J. Powell, and D. R. Penn, Calculations of electron inelastic mean free paths. XII. Data for 42 inorganic compounds over the 50 eV to 200 keV range with the full Penn algorithm, *Surf. Interface Anal.* **43**, 689 (2011); C. J. Powell, A. Jablonski, I. S. Tilinin, S. Tanuma, and D. R. Penn, Surface sensitivity of Auger-electron spectroscopy and x-ray photoelectron spectroscopy, *J. Electron Spectros. Relat. Phenom.* **98-99**, 1 (1999).
- [63] M. B. Trzaskovskaya, and V. G. Yarzhevsky, Dirac-Fock photoionization parameters for HAXPES applications, *At. Data Nucl. Data Tables* **119**, 99 (2018).
- [64] M. Maniraj, S. W. D'Souza, A. Rai, D. L. Schlager, T. A. Lograsso, A. Chakrabarti, and S. R. Barman, Unoccupied electronic structure of Ni<sub>2</sub>MnGa ferromagnetic shape memory alloy, *Solid State Commun.* **222**, 1 (2015).
- [65] C. Fadley, Progress in quantitative surface analysis by x-ray photoelectron spectroscopy: Current status and perspectives, *J. Electron Spectrosc. Relat. Phenom.* **178-179**, 2 (2010).
- [66] Y. Takata, Y. Kayanuma, M. Yabashi, K. Tamasaku, Y. Nishino, D. Miwa, Y. Harada, K. Horiba, S. Shin, S. Tanaka, E. Ikenaga, K. Kobayashi, Y. Senba, H. Ohashi, and T. Ishikawa, Recoil effects of photoelectrons in a solid, *Phys. Rev. B* **75**, 233404 (2007); Y. Takata, Y. Kayanuma, S. Oshima, S. Tanaka, M. Yabashi, K. Tamasaku, Y. Nishino, M. Matsunami, R. Eguchi, A. Chainani, M. Oura, T. Takeuchi, Y. Senba, H. Ohashi, S. Shin, and T. Ishikawa, Recoil Effect of Photoelectrons in the Fermi Edge of Simple Metals, *Phys. Rev. Lett.* **101**, 137601 (2008).
- [67] A. Ayuela, J. Enkovaara, K. Ullakko, and R. M. Nieminen, Structural properties of magnetic Heusler alloys, *J. Phys.: Condens. Matter* **11**, 2017 (1999).
- [68] S. L. Dudarev, G. A. Botton, S. Y. Savrasov, C. J. Humphreys, and A. P. Sutton, Structural properties of magnetic Heusler alloys, *Phys. Rev. B* **57**, 1505 (1998).
- [69] J. Janovec, M. Zeleny, O. Heczko, and A. Ayuela, Localization versus delocalization of d-states within the Ni<sub>2</sub>MnGa Heusler alloy, *Sci. Rep.* **12**, 20577 (2022).
- [70] M. Zeleny, P. Sedlak, O. Heczko, H. Seiner, P. Vertat, M. Obata, T. Kotani, T. Oda, and L. Straka, Effect of electron localization in theoretical design of Ni-Mn-Ga based magnetic shape memory alloys, *Mater. Des.* **209**, 109917 (2021).
- [71] T. Koubský, P. Sedláč, H. Seiner, J. Fojtíková, M. Obata, T. Odac, and L. Kalvodaa, Ab Initio Study of Martensitic Transition in Ni<sub>2</sub>MnGa, *Acta Phys. Pol. A* **134**, 804 (2018).
- [72] U. Devarajan, S. E. Muthu, S. Arumugam, S. Singh, and S. R. Barman, Investigation of the influence of hydrostatic pressure on the magnetic and magnetocaloric properties of Ni<sub>2-x</sub>Mn<sub>1-x</sub>Ga (X= 0, 0.15) Heusler alloys, *J. Appl. Phys.* **114**, 053906 (2013).
- [73] K. Ooiwa, K. Endo, and A. Shinogi, A structural phase transition and magnetic properties in a Heusler alloy Ni<sub>2</sub>MnGa, *J. Magn. Magn. Mater.* **104-107**, 2011 (1992).
- [74] S. Singh, S. W. D'Souza, J. Nayak, L. Caron, E. Suard, S. Chadov, and C. Felser, Effect of platinum substitution on the structural and magnetic properties of Ni<sub>2</sub>MnGa ferromagnetic shape memory alloy, *Phys. Rev. B* **93**, 134102 (2016).
- [75] S. W. D'Souza, T. Roy, S. R. Barman, and A. Chakrabarti, Magnetic properties and electronic structure of Mn-Ni-Ga magnetic shape memory alloys, *J. Phys.: Condens. Matter* **26**, 506001 (2014).
- [76] A. Singh, H. Y. Huang, Y. Y. Chin, Y. F. Liao, T. C. Huang, J. Okamoto, W. B. Wu, H. J. Lin, K. D. Tsuei, R. P. Wang, F. M. F. de Groot, C. N. Kuo, H. F. Liu, C. S. Lue, C. T. Chen, D. J. Huang, and A. Chainani, Electronic structure investigation of a charge density wave coupled to a metal-to-metal transition in Ce<sub>3</sub>Co<sub>4</sub>Sn<sub>13</sub>, *Phys. Rev. B* **98**, 235136 (2018).
- [77] B. Dardel, D. Malterre, M. Grioni, P. Weibel, Y. Baer, and F. Levy, Unusual Photoemission Spectral Function of Quasi-One-Dimensional Metals, *Phys. Rev. Lett.* **67**, 3144 (1991).
- [78] B. Dardel, M. Grioni, D. Malterre, P. Weibel, Y. Baer, and F. Levy, Spectroscopic signatures of phase transitions in a charge-density-wave system: 1T-TaS<sub>2</sub>, *Phys. Rev. B* **46**, 7407 (1992).
- [79] J. Matsuno, A. Fujimori, L. F. Mattheiss, R. Endoh, and S. Nagata, Photoemission and band-calculation studies of the charge-density wave in CuV<sub>2</sub>S<sub>4</sub>, *Phys. Rev. B* **64**, 115116 (2001).
- [80] T. Yokoya, T. Kiss, A. Chainani, S. Shin, and K. Yamaya, Role of charge-density-wave fluctuations on the spectral function in a metallic charge-density-wave system, *Phys. Rev. B* **71**, 140504(R) (2005).
- [81] C. A. Balseiro, P. Schlottmann, and F. Yndurain, Coexistence of charge-density waves and magnetic order, *Phys. Rev. B* **21**, 5267 (1980).
- [82]  $[w \times f(E, T) \times [|E - E_0|^\alpha h(E - E_0) + |E'_0 - E|^\alpha h(E'_0 - E)]] \otimes (E, \sigma)$ , where  $E_0$  ( $E'_0$ ) is the threshold energy of the left (right) branch of the power law spectral function,  $h$  denotes a unit step function,  $\alpha$  is the exponent of the power-law function, and  $w$  is a multiplicative factor.  $f(E, T)$  represents the Fermi function at temperature  $T$ .
- [83] G. Kresse and J. Furthmüller, Efficient iterative schemes for ab initio total-energy calculations using a plane-wave basis set, *Phys. Rev. B* **54**, 11169 (1996); G. Kresse and D. Joubert, From ultrasoft pseudopotentials to the projector augmented-wave method, *ibid.* **59**, 1758 (1999).
- [84] J. P. Perdew, K. Burke, and M. Ernzerhof, From Ultrasoft Pseudopotentials to the Projector Augmented-Wave Method, *Phys. Rev. Lett.* **77**, 3865 (1996).
- [85] H. J. Monkhorst and J. D. Pack, Special points for Brillouin-zone integrations, *Phys. Rev. B* **13**, 5188 (1976).
- [86] A. Gloskovskii, G. Stryganyuk, G. H. Fecher, C. Felser, S. Thiess, H. Schulz-Ritter, W. Drube, G. Berner, M. Sing, R. Claessen, and M. Yamamoto, Magnetometry of buried layers: Linear magnetic dichroism and spin detection in angular resolved hard x-ray photoelectron spectroscopy, *J. Electron Spectrosc. Relat. Phenom.* **185**, 47 (2012).

- [87] D. L. Schlager, Y. L. Wu, W. Zhang, and T. A. Lograsso, Chemical segregation during bulk single crystal preparation of Ni-Mn-Ga ferromagnetic shape memory alloys, *J. Alloys Compd.* **312**, 77 (2000).
- [88] R. S. Dhaka, S. W. D'Souza, M. Maniraj, A. Chakrabarti, D. L. Schlager, T. A. Lograsso, and S. R. Barman, Photoemission study of the (100) surface of Ni<sub>2</sub>MnGa and Mn<sub>2</sub>NiGa ferromagnetic shape memory alloys, *Surf. Sci.* **603**, 1999 (2009).
- [89] S. R. Barman and D. D. Sarma, Electronic structures of gallium and indium across the solid-liquid transition, *Phys. Rev. B* **51**, 4007 (1995).
- [90] D. A. Shirley, High-resolution x-ray photoemission spectrum of the valence bands of gold, *Phys. Rev. B* **5**, 4709 (1972).
- [91] A. Chakrabarti, M. Siewert, T. Roy, K. Mondal, A. Banerjee, M. E. Gruner, and P. Entel, Influence of Ni doping on the electronic structure of Ni<sub>2</sub>MnGa, *Phys. Rev. B* **88**, 174116 (2013); A. T. Zayak, P. Entel, K. M. Rabe, W. A. Adeagbo, and M. Acet, Anomalous vibrational effects in nonmagnetic and magnetic Heusler alloys, *ibid.* **72**, 054113 (2005).
- [92] A. Chakrabarti, C. Biswas, S. Banik, R. S. Dhaka, A. K. Shukla, and S. R. Barman, Influence of Ni doping on the electronic structure of Ni<sub>2</sub>MnGa, *Phys. Rev. B* **72**, 073103 (2005).
- [93] K. Momma and F. Izumi, VESTA 3 for three-dimensional visualization of crystal, volumetric and morphology data, *J. Appl. Crystallogr.* **44**, 1272 (2011).
- [94] H. Seiner, O. Heczko, P. Sedlák, L. Bodnárová, M. Novotný, J. Kopecek, and M. Landa, Combined effect of structural softening and magneto-elastic coupling on elastic coefficients of Ni-Mn-Ga austenite, *J. Alloys Compd.* **577**, S131 (2013).
- [95] J. Worgull, E. Petti, and J. Trivisonno, Behavior of the elastic properties near an intermediate phase transition in Ni<sub>2</sub>MnGa, *Phys. Rev. B* **54**, 15695 (1996).
- [96] Q.-M. Hu, C.-M. Li, R. Yang, S. E. Kulkova, D. I. Bazhanov, B. Johansson, and L. Vitos, Site occupancy, magnetic moments, and elastic constants of off-stoichiometric Ni<sub>2</sub>MnGa from first-principles calculations, *Phys. Rev. B* **79**, 144112 (2009).